Calibration and Verification of Pointing and Tracking System for Smallsat Optical Communication Terminal

Francesco Sansone*
Stellar Project s.r.l., Padova, Italy

Francesco Branz†
University of Padova, Padova, Italy

Andrea Vettor‡ and Edoardo Birello§
Stellar Project s.r.l., Padova, Italy

Gian Paolo Guizzo¶
Guizzo Space s.r.l.s., San Vito al Tagliamento, Italy

Riccardo Antonello‖
University of Padova, Vicenza, Italy

Alessandro Francesconi**
Stellar Project s.r.l., Padova, Italy
University of Padova, Padova, Italy

This paper presents the experimental verification of the pointing and tracking system of the flight model of an optical communication terminal for small satellites. The terminal, called LaserCube, fits in two CubeSat units and is conceived to operate on–board spacecraft starting from the 6 U form factor. The terminal is provided with a dual stage pointing system, composed by a coarse pointing mechanism used to orient the optical head and a fast–steering mirror for the fine pointing of the received and transmitted lasers. The coarse pointing mechanism is based on the parallel platform configuration and alone can provide 50 µrad rms pointing accuracy when operating in conjunction with a beacon laser sent by a remote terminal and used for feedback. The control algorithm operates the two pointing stages synergically, targeting an overall pointing accuracy of 10 µrad rms while rejecting the disturbances coming from the satellite bus. The pointing system of the LaserCube flight model has been calibrated and experimentally verified in laboratory conditions that replicate real operational scenarios for what concerns the beacon signal attenuation and the disturbances generated by the host satellite. A dedicated setup was used to directly measure the pointing error and asses the system performance.

*Lead Engineer
†Reasearch Associate, Department of Industrial Engineering, corresponding author: francesco.branz@unipd.it
‡Optical Engineer
§Optical Engineer
¶CEO and Electronic Engineer
‖Assistant Professor, Department of Management and Engineering
**Managing Director; Associate Professor, Department of Industrial Engineering

Acronyms

ADU	=	Actuators Driver Unit
APD	=	Avalance Photodiode
BCN	=	Beacon
DL	=	Downlink
ELU	=	Electronic Unit
EM	=	Engineering Model
EO	=	Earth Observation
FM	=	Flight Model
$FPGA$	=	Field Programmable Gate Array
FSM	=	Fast Steering Mirror
IOD	=	In–Orbit Demonstration
ISL	=	Inter–Satellite Link
LC	=	LaserCube
LDU	=	Laser Driver Unit
MOS	=	Miniature Optical Subsystem
MTS	=	Miniature Telecom Subsystem
OMU	=	Opto–Mechanical Unit
PAT	=	Pointing, Acquisition and Tracking
PCB	=	Printed Circuit Board
$PCCU$	=	Payload Control and Conditioning Unit
$PCDU$	=	Power Conversion and Distribution Unit
PCS	=	Payload Control System
PID	=	Proportional–Integral–Derivative
PSD	=	Position Sensitive Detector
QD	=	Quadrant Detector
RF	=	Radio Frequency
SAR	=	Synthetic Aperture Radar
SG	=	Strain Gauge
$SPIN$	=	Stabilization and Pointing Instrument for Nanosatellites
$SWaP$	=	Size, Weight and Power
TLC	=	Telecom
TMU	=	Telecom Management Unit

I. Introduction

With thousands of small satellites launches forecasted for the next decade, a huge increase in the generation of space–borne data to be transmitted to the ground is expected. This exceptionally large amount of data may overwhelm the current capabilities of small satellites telecommunication subsystems based on radio technologies. In this context, the space community has recently shown an increasing interest for satellite optical communications. These systems can provide a considerably increased link capacity in both downlink (DL) and intersatellite link (ISL) scenarios, if compared to traditional RF systems. Optical communications are also characterized by improved security (immunity from jamming or interception) that can be further enhanced by the application of quantum encryption techniques. Moreover, there are currently no regulations for optical frequency bands allocation, while radio frequency filing is becoming an issue.

Many efforts have been devoted recently to the miniaturization of critical technologies that are needed for the realization of low–mass, low–power consumption laser communication terminals suitable for nano and micro satellites

Table 1 Summary of lasercom terminals for small satellites with main specifications.

	Mass [kg]	**Pow.** [W]	**Accur.** [µrad]	**Ref.**
OCSD	0.3†	22	140	[1, 2]
NODE (CLICK–A)	1.2	15	16	[3, 4]
CLICK–B/–C	1.7	20†	26	[5–7]
OSIRIS4CubeSat	0.4	8.5	<100†	[8, 9]
Fibertek LCT	2	20	20	[10, 11]
CubeCAT	1	15	<100†	[12]
LaserCube	**1.8**	**26**	**<10**	

† presumed

(see Tab. 1). A critical aspect of laser communication is the extremely accurate pointing accuracy that is needed to correctly point the very narrow beams (in the order of 10–100 µrad). Proposed laser communication terminals for small satellites typically exploit some form of fine pointing systems based on tiltable mirrors with high rotational accuracy but very limited range (< 1 deg), delegating coarse pointing tasks to the satellite bus. Over the last years, Stellar Project [13] and their partners have developed LaserCube, a laser communication terminal suitable for nano and micro satellites with dedicated coarse pointing capabilities. Two configurations of LaserCube have been developed, either optimized for DL or ISL operations, with minor differences in the system design, providing up to 1 Gbps DL and 100 Mbps ISL. The adoption of LaserCube–DL terminals may result particularly advantageous for small satellites dedicated to Earth Observation (EO) missions, either in the optical (both visible and infrared) and radio (Synthetic Aperture Radar, SAR) bands. The increased downlink capability compared to traditional RF telecom systems allows for a larger amount of data transmitted to the ground in a single pass over a ground station, leading to a significant decrease of data latency. Moreover, the adoption of the optical band may lead to the use of optical ground stations supporting high–throughput optical downlinks with reduced aperture (0.5–1 m) with respect to their radio counterparts (typically in the order of few meters). The exploitation of LaserCube–ISL terminals to transmit data between satellites within a constellation will further contribute to reduce the latency of data, since they can be routed from satellite to satellite until a ground station is within sight, as opposed to the classic store–and–forward technique (also reducing the amount of ground station necessary to support EO constellations).

This paper presents the calibration and experimental verification of the Pointing, Acquisition and Tracking (PAT) system of the LaserCube–Downlink Flight Model (LC–DL–FM). The first LaserCube–DL flight model was launched in June 2021 on board the D–Orbit ION Satellite Carrier 003 and its In–Orbit Demonstration (IOD) mission is ongoing at the time of writing. In Sec. II a brief description of the terminal is provided, with focus on the PAT system. Section III describes the calibration process and the experimental verification; finally, conclusions are drawn in Sec. IV.

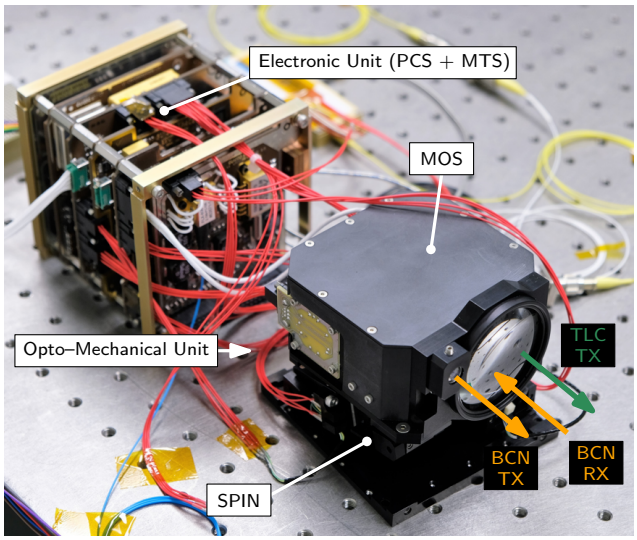

Fig. 1 LaserCube–Downlink Flight Model.

II. LaserCube–DL Terminal Description

The LaserCube–DL optical communication terminal is composed by two main subunits, namely the Opto–Mechanical Unit (OMU) and the Electronic Unit (ELU); the terminal is shown in Fig. 1.

The OMU features two subsystems: the Stabilization and Pointing System for Nanosatellites (SPIN) and the Miniature Optical Subsystem (MOS). The SPIN is a 2–DoF (rotational) coarse pointing mechanism based on the parallel platform configuration (technology patented by Stellar Project [14]), which is used to orient the optical axis of the MOS main lens with an accuracy in the order of 50 µrad. The platform is actuated by means of two linear piezoelectric motors with sub–micron resolution. The mechanism is provided with a launch lock device whose purpose is to increase the system stiffness during the launch phase. The MOS features a refractive telescope with 42 mm aperture, a Fast Steering Mirror (FSM) for fine pointing actuation (resolution in the order of 1 µrad) and a Quadrant Detector (QD) that is used to measure the pointing error between the main lens boresight and the incoming beacon direction. The field of view of the optical system is ±1 deg.

The ELU is composed by a stack of PC/104 PCBs arranged into the Miniature Telecom Subsystem (MTS) and the Payload Control Subsystem (PCS).

The MTS comprises the Laser Driver Unit (LDU) and the Telecom Management Unit (TMU). The LDU features the driver circuitry for the two laser sources (beacon and telecom) and their dedicated thermo–electric coolers. The 1550 nm telecom laser is operated as continuous wave and modulation is realized through a pigtailed amplitude optical modulator, which receives the telecom laser carrier as input. The modulator is driven by the TMU at GHz frequencies, for bitrates in the range of 0.5–1 Gbps, and its optical output is then connected to the MOS. The TMU includes the FPGA responsible for generation of RF modulation signals for the optical modulator.

The PCS is composed by four PCBs. The Payload Control and Conditioning Unit (PCCU) hosts the microcontroller

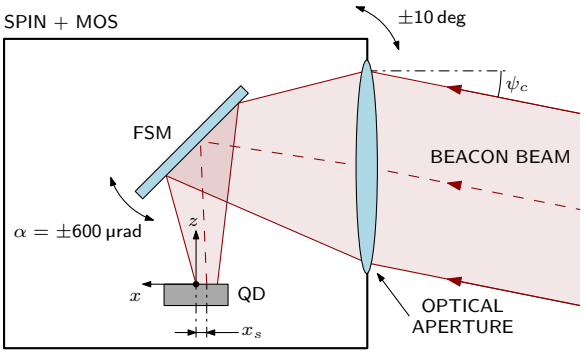

Fig. 2 The elements of the LaserCube dual stage pointing system: SPIN, MOS, FSM and QD. The main quantities involved in the measurement of the azimuth angle are reported (ψ_c, x_s and α).

that executes the lasercom terminal main software; the PCCU manages all payload functionalities except those strictly related to telecom laser modulation, including execution of the PAT control algorithms, system monitoring and generation of housekeeping data, communication with the host satellite bus for telecommands and telemetry, acquisition and conditioning of the beacon detector as well as the actuators encoders. The data link is based on CAN Bus. The Actuator Driver Unit (ADU) generates the driving signals for both the SPIN linear actuators and the FSM piezo tip–tilt platform. The Power Conversion and Distribution Unit (PCDU) generates the voltage levels that are required by the different elements of the terminal. The accepted input power line is 16–40 V unregulated. To ensure compatibility with different platforms, the PCS also features an additional, customizable interface board with dedicated power and data connectors that is used if the electrical bus of the host spacecraft is not based on the PC/104 standard. In general, two lines (nominal and redundant) are available for both power and data. Each LaserCube unit has a SWaP of 2 U / 2 kg / up to 25 W (DL) and 30 W (ISL), thus being suitable for small satellites starting from the 6 U form factor, and larger. The coarse pointing capability provided by SPIN is a key factor towards easing the LaserCube compatibility with small platforms, since it relieves the satellite from very precise pointing tasks.

A. PAT system

The LaserCube Pointing, Acquisition and Tracking (PAT) system is composed by the SPIN pointing mechanism (primary stage), the MOS FSM (secondary stage) and the QD (see Fig. 2). The PAT system operates in two main modes: (1) acquisition (seeking) mode and (2) tracking mode. In the first case, an open loop trajectory is commanded to the pointing mechanism in order to detect an incoming beam. Several types of trajectories can be implemented to completely sweep the operational space in terms of elevation and azimuth, but one of the most efficient is the spiral trajectory [15]. As soon as the incoming beacon beam is detected, the PAT switches to tracking mode and aligns the optical axis of the MOS with the beacon direction by keeping the beam spot at the center of the QD sensitive area. In other words, the latter provides the pointing error information to the system controller when a beacon beam from a remote terminal is available. The QD measures the spot position on the sensing element $[x_s, y_s]$, which is then

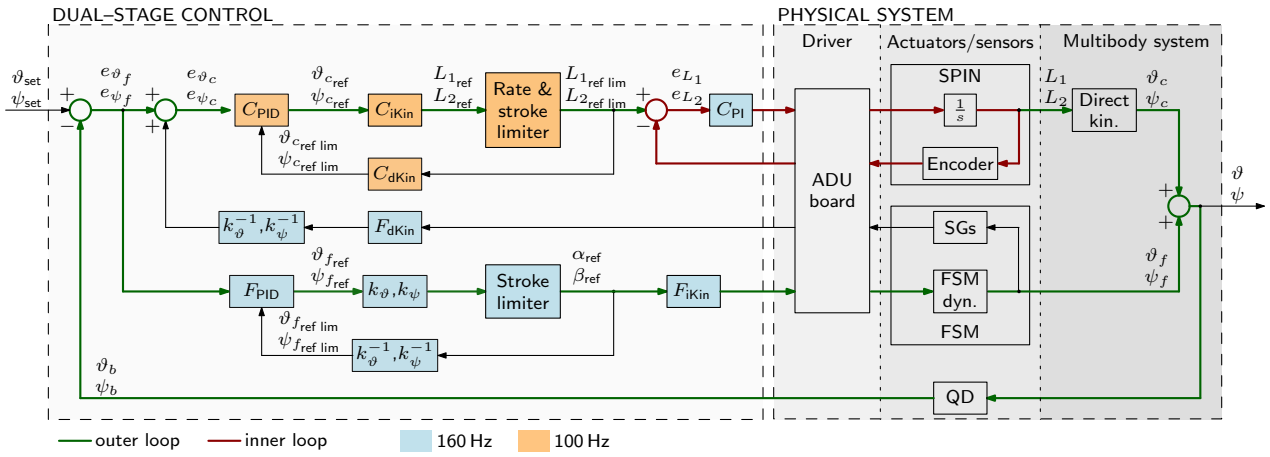

Fig. 3 LaserCube dual stage control architecture.

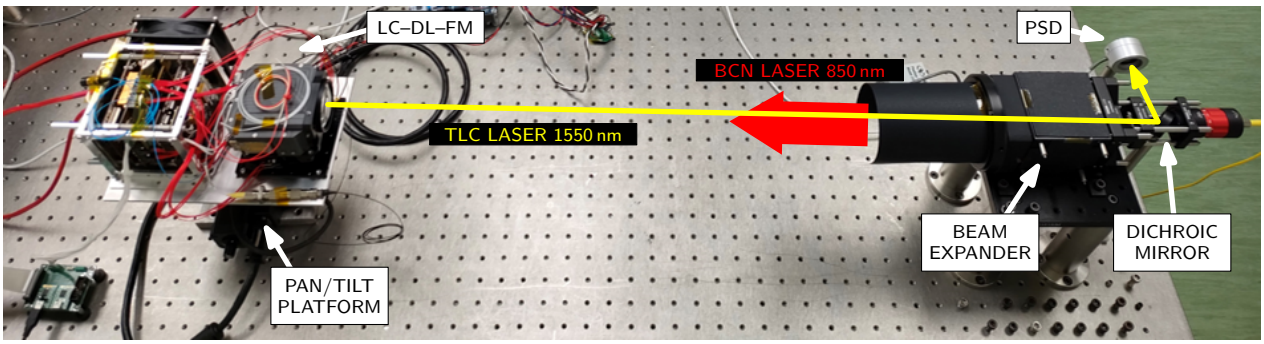

Fig. 4 Test setup: (1) LaserCube–Downlink FM (left) mounted on a pan–tilt platform, (2) beam expander used to generate the beacon beam, (3) PSD detector used to measure the pointing error of the telecom laser transmitted by LaserCube.

correlated to the incoming beacon direction $[\vartheta, \psi]$ through the following equations (see Fig. 2):

$$\begin{aligned} \psi &= \frac{x_s}{f} = \psi_c + 2\frac{f_{FSM}}{f}\alpha \\ \vartheta &= \frac{y_s}{f} = \vartheta_c + \sqrt{2}\frac{f_{FSM}}{f}\beta \end{aligned} \tag{1}$$

where $[\vartheta_c, \psi_c]$ are the attitude angles of the coarse pointing system relative to the received beacon beam, f and f_{FSM} are, respectively, the focal length of the MOS main lens and a quantity that represents the distance between the FSM centre and the QD centre (i.e., the optical lever of the FSM), both known by geometry, and $[\alpha, \beta]$ are the mechanical angles of the FSM.

The control system architecture is depicted in Fig. 3 and it is based on the sensitivity decoupled method proposed in [16] and [17]. The method enables a separate design for the controllers of the primary and secondary stage, while guaranteeing that the sensitivity of the resulting dual–stage control system is the product of the sensitivities of the two independent designs. A detailed description of the control algorithm can be found in [18]. In Fig. 3, blue blocks are executed at 160 Hz and orange blocks at 100 Hz.

The outer control loop in Fig. 3 computes the commands for both the primary and secondary stages based on the

pointing error calculated as the difference between the reference setpoint $[\vartheta_{set}, \psi_{set}]$ and the incoming beacon direction $[\vartheta, \psi]$, measured by the QD. The setpoint is typically zero for both angles since the MOS optical axis shall be nominally aligned with the incoming beacon beam. PID controllers are used for the generation of the control commands for both the primary (C_{PID}) and secondary (F_{PID}) stages. Inverse kinematics relations C_{iKin} convert the angular commands of the primary stage into elongation values for the linear actuators. Stroke and rate limiters are applied to the commands generated by the C_{PID} and direct kinematics C_{dKin} is used to estimate the current platform orientation from the limited setpoints fed to the linear motors. The inner control loop drives the primary stage linear actuators to the positions required by the outer control loop, exploiting the feedback given by the linear encoder measurements.

Considering the secondary stage, the PID controller F_{PID} generates the angular setpoint for the FSM; scale factors k_ϑ and k_ψ manage the conversion from the mirror mechanical tilt $[\alpha, \beta]$ and the optical deflection of the laser beams. This is described in detail in Sec. III.B.2. Strain Gauges (SG) measurements provide the current orientation of the FSM, which is taken into account by the controller of the coarse pointing stage allowing the two pointing stages to work synergically.

III. PAT System Verification

This section presents the experimental activities conducted on the PAT system of the Flight Model (FM) of LaserCube–DL with the goal of calibrating the system and verifying the beacon acquisition procedure and the transition from search mode to tracking mode. Calibrations involved the QD, to properly correlate the sensor outputs with attitude angles, and the FSM, to estimate the relation between the commanded angles and the resulting beam deflection.

A. Test Setup

The verification of the PAT functionalities and performances took place in laboratory. The test setup (Fig. 4) is assembled on a large optical table that guarantees high structural stiffness and rigidity. Beside the LaserCube model, a number of components are required to execute the calibration procedures and the test campaign. The test setup comprises:

- The FM of LaserCube–DL, composed by both subunits (OMU and ELU).
- The pan/tilt platform for the simulation of attitude jitter; the FM is mounted on top of the platform.
- A 850 nm laser source and driver with wavelength and temperature stabilization, to emit the beacon beam used as the reference for alignment.
- A beam expander with collimator, to widen the beacon beam and completely illuminate the optical aperture of LaserCube, thus emulating a faraway beam source (i.e., satellite or ground station).
- A Position Sensitive Detector (PSD) Conex–PSD10GE, with wavelength range 800–1700 nm, to provide an external measurement of the LaserCube alignment error w.r.t. the beacon direction.

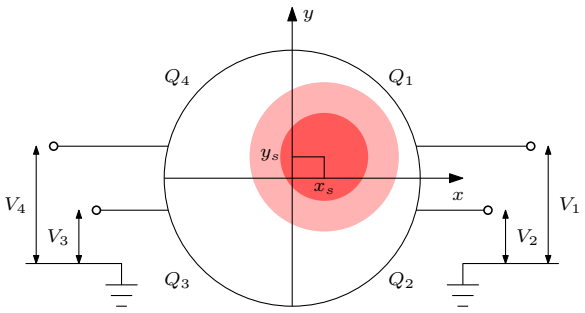

Fig. 5 Schematic representation of the active area of the QD with focused beacon beam (red spot); each quadrant outputs a voltage that is proportional to the sensed light intensity (four channels in total).

- A laboratory computer to operate LaserCube through CAN bus, to control the pan/tilt platform and to record the PSD output data.

B. System Calibration

In this section, the calibration of the quadrant detector outputs and of the FSM scale factors is described.

1. Quadrant Detector Calibration

The QD is used to measure the angles $[\vartheta, \psi]$ between the boresight direction of LaserCube and the incoming beacon beam sent by a remote terminal that emulates a ground station or satellite. The incoming beam is focused on the QD by the main lens of the MOS. The circular active area of the QD is split in four quadrants that output a voltage value proportional to the intensity of the incident light. The beam is reflected midcourse by the FSM used for fine pointing corrections, as shown in Fig. 2. Considering Fig. 5, the relationship between the laser spot position $[x_s, y_s]$ on the QD active area, with respect to the detector centre, and the output voltages $\bar{V} = [V_1, \ldots, V_4]$ is given by Eq. 3 and Eq. 2, where k_1 and k_2 are scale factors with dimension of metres:

$$\begin{aligned} x_s &= k_1 F_x(\bar{V}) \\ y_s &= k_2 F_y(\bar{V}) \end{aligned} \tag{2}$$

$$\begin{aligned} F_x(\bar{V}) &= \frac{(V_1 + V_2) - (V_3 + V_4)}{V_1 + V_2 + V_3 + V_4} \\ F_y(\bar{V}) &= \frac{(V_1 + V_4) - (V_2 + V_3)}{V_1 + V_2 + V_3 + V_4} \end{aligned} \tag{3}$$

Note that in Eq. 3 the values of F_x and F_y are normalized by the sum of voltages on all four channels of the QD in order to remove the dependency on the intensity of the total incoming light. The attitude angles $[\vartheta, \psi]$ are correlated to the

QD outputs $\bar{V} = [V_1, \ldots, V_4]$ by Eq. 4:

$$\begin{aligned} \psi &= \frac{x_s}{f} = \frac{k_1 F_x(\bar{V})}{f} \\ \vartheta &= \frac{y_s}{f} = \frac{k_2 F_y(\bar{V})}{f} \end{aligned} \tag{4}$$

The goal of the calibration procedure is the experimental estimation of k_1 and k_2. The adopted procedure is the following:

1) Manual alignment of the OMU with the beacon beam so that the laser spot is focused approximately at the center of the QD by the MOS main lens.
2) Measurement of the initial QD output voltages $\bar{V}_0 = [V_{10}, \ldots, V_{40}]$.
3) Calculation of the initial values of $F_x(\bar{V}_0)$, $F_y(\bar{V}_0)$ with Eq. 3.
4) Imposition of n known deviation angles $[\vartheta_n, \psi_n]$ to the incoming beacon beam through the deflection of the FSM by commanding the mechanical angles $[\alpha_n, \beta_n]$; the imposed angles are measured by the FSM strain gauges with an accuracy of 10 µrad rms.
5) For each combination of imposed deviation angles $[\vartheta_n, \psi_n]$:
    1) Measurement of the QD output voltages $\bar{V}_n = [V_{1n}, \ldots, V_{4n}]$.
    2) Calculation of $F_x(\bar{V}_n)$ and $F_y(\bar{V}_n)$ with Eq. 3.
    3) Calculation of the variation of F_x and F_y w.r.t. the initial value:

$$\begin{aligned} \Delta F_x(\bar{V}_n) &= F_x(\bar{V}_n) - F_x(\bar{V}_0) \\ \Delta F_y(\bar{V}_n) &= F_y(\bar{V}_n) - F_y(\bar{V}_0) \end{aligned} \tag{5}$$

    4) Calculation of x_{s_n} and y_{s_n} with the following relations given by geometry:

$$\begin{aligned} x_{s_n} &= 2\alpha_n f_{FSM} \\ y_{s_n} &= \sqrt{2}\beta_n f_{FSM} \end{aligned} \tag{6}$$

    Note the factor 2 in the $\alpha \rightarrow x_s$ relation (rotation in the X–Z plane of Fig. 2) and the factor $\sqrt{2}$ in the $\beta \rightarrow y_s$ relation (rotation in the Y–Z plane of Fig. 2).
6) Estimation of the values of k_1 and k_2 as the slopes of the linear relations between x_s and ΔF_x, and between y_s and ΔF_y. The values resulting from the linear regression between the n couples of measurements $[x_{s_n}, \Delta F_x(\bar{V}_n)]$

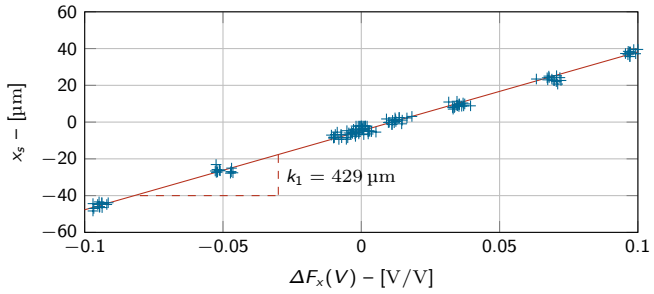

(a) Linear relation between x_s and $\Delta F_x(\bar{V})$.

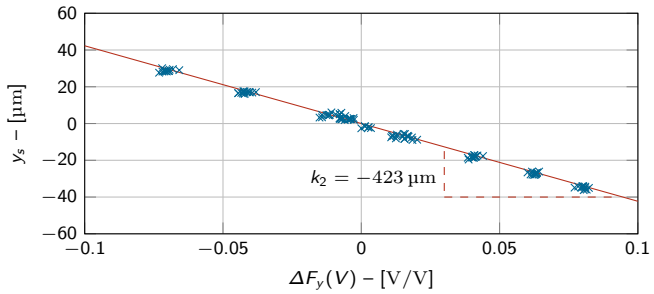

(b) Linear relation between y_s and $\Delta F_y(\bar{V})$.

Fig. 6 Results of the QD calibration. Relation between the QD voltage functions, $\Delta F_x(\bar{V})$ and $\Delta F_y(\bar{V})$, and the spot position $[x_s, y_s]$ on the sensitive area. The slope of the linear regressions are the scale factors, k_1 and k_2.

and $[y_{s_n}, \Delta F_y(\bar{V}_n)]$ are ($R^2 = 0.99$):

$$k_1 = \ 4.29 \times 10^{-4}\,\mathrm{m}$$

$$k_2 = -4.23 \times 10^{-4}\,\mathrm{m}$$

The calibration results are presented in Fig. 6, which shows the linear regression between x_s and ΔF_x, y_s and ΔF_y. Figure 7 compares the values of x_s and y_s as calculated after calibration with Eq. 6 from the FSM strain gauges measurements and with Eq. 2 from the QD outputs.

The calibration of k_1 and k_2 enables the estimation of the uncertainty on the measured attitude angles $[\vartheta, \psi]$ due to the QD noise. A static test allows to quantify the contribution of the sensor noise on the angle estimates. The OMU is aligned with the beacon beam sent through the beam expander and the QD outputs have been recorded in static conditions. Then, $[\vartheta, \psi]$ is calculated according to Eq. 4 and their standard deviations $[\sigma_\vartheta, \sigma_\psi]$ are calculated and used to quantify the uncertainty on $[\vartheta, \psi]$. The resulting values are $\sigma_\vartheta = 2.0\,\mu\mathrm{rad}$ and $\sigma_\psi = 2.2\,\mu\mathrm{rad}$ respectively. The measured values of $[\vartheta, \psi]$ are shown in Fig. 8 with a scatter plot in the ψ–ϑ domain (left) and with histograms representing the empirical probability distribution function of ψ and ϑ (right).

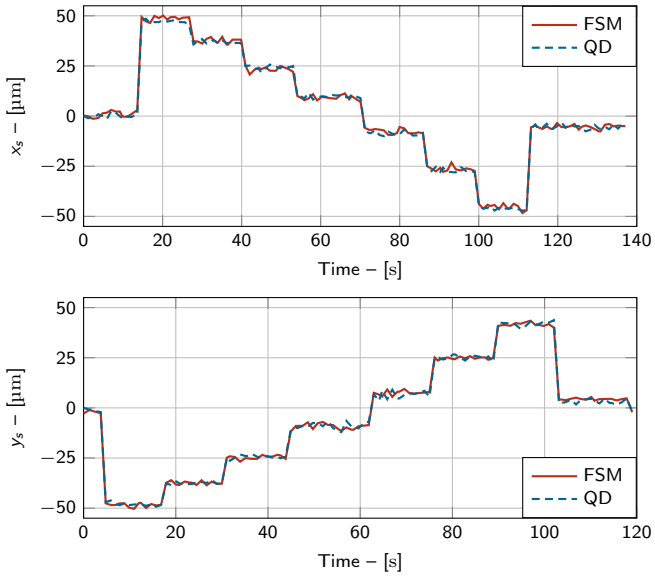

Fig. 7 Comparison of values of x_s and y_s obtained from the FSM strain gauges measurements and the QD outputs, after calibration.

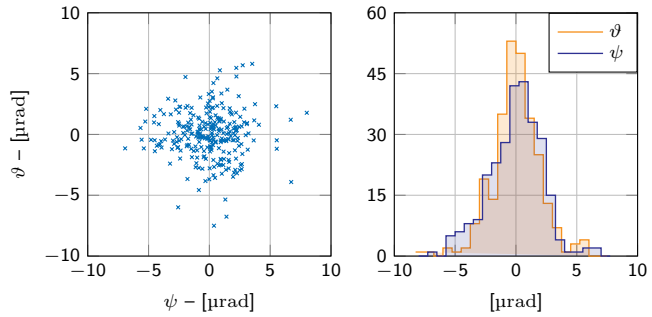

Fig. 8 Estimation of elevation ϑ and azimuth ψ from the quadrant detector outputs, in static condition. Plot in the ψ–ϑ domain (left) and empirical probability distribution (right).

2. *Fine Pointing System Calibration*

In the control scheme presented in Fig. 3, the FSM finely compensates for the SPIN attitude error; it acts as the secondary stage and its action is summed to that of the primary stage. In order to correctly actuate the FSM, it is necessary to determine the correlation coefficients k_ϑ and k_ψ between the SPIN attitude error angles $[\vartheta, \psi]$, as measured by the QD, and the mechanical angles $[\alpha, \beta]$, imposed to the FSM and measured by the strain gauges.

A procedure similar to that presented in Sec. III.B.1 is adopted for this calibration. Equation 7 correlates the mechanical angles $[\alpha, \beta]$ imposed by the FSM to the variations of the angles of incidence $[\Delta\vartheta, \Delta\psi]$ of the incoming beam on the QD:

$$\begin{aligned} \alpha &= \frac{k_\psi}{2}\Delta\psi \\ \beta &= \frac{k_\vartheta}{\sqrt{2}}\Delta\vartheta \end{aligned} \tag{7}$$

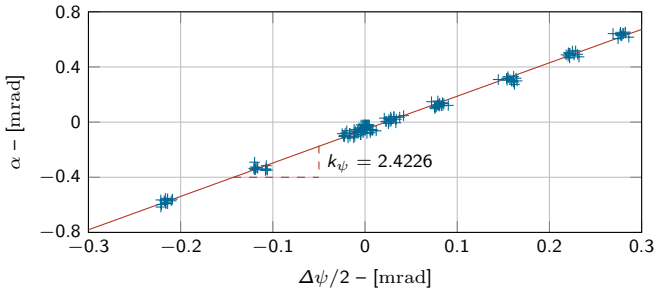

(a) Linear relation between α and $\Delta\psi$.

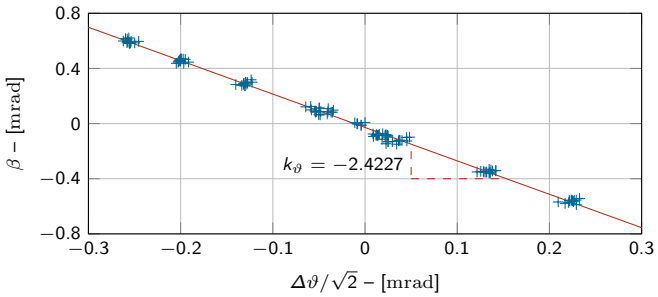

(b) Linear relation between β and $\Delta\vartheta$.

Fig. 9 Results of the FSM calibration. Relation between the FSM mechanical angles, α and β, and the variations of the angles of incidence $[\Delta\vartheta, \Delta\psi]$ on the QD. The slope of the linear regression provides the values of the scale factors, k_ψ and k_ϑ.

where k_ϑ and k_ψ are the non–dimensional scale factors to be determined experimentally.

The variations $[\Delta\vartheta, \Delta\psi]$ are computed from the QD outputs by Eq. 8, where f is the focal length of the MOS main lens:

$$\begin{aligned} \Delta\psi &= \frac{\Delta x_s}{f} = \frac{k_1}{f}\left[F_x(\bar{V}) - F_x(\bar{V}_0)\right] \\ \Delta\vartheta &= \frac{\Delta y_s}{f} = \frac{k_2}{f}\left[F_y(\bar{V}) - F_y(\bar{V}_0)\right] \end{aligned} \tag{8}$$

The values of k_ψ and k_ϑ are estimated through linear regression between β and $\Delta\vartheta/\sqrt{2}$, and between α and $\Delta\psi/2$. The division by 2 on azimuth and by $\sqrt{2}$ on elevation is applied to take into account the law of reflection that relates mechanical and optical angles of the FSM. The coefficients k_ψ and k_ϑ are given by the slope of the linear regression, and their values are, respectively, 2.4226 and −2.4227 (see Fig. 9). In Fig. 10 the comparison between the measures of the mechanical angles $[\alpha, \beta]$ obtained directly from the strain gauges and indirectly from QD readings through Eq. 7 is presented.

C. Acquisition Procedure

LaserCube enters in acquisition (seeking) mode when no incoming beacon beam is detected. The seeking procedure consists in the OMU coarse pointing system scanning its field of regard in search of the beacon laser sent by an optical

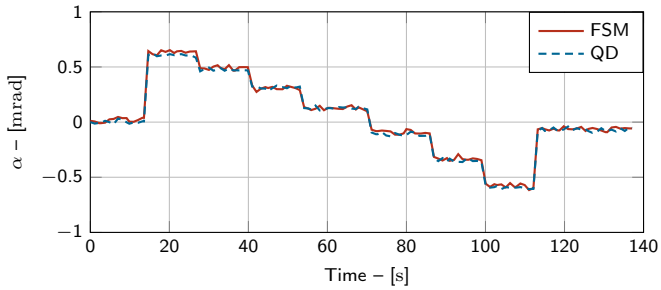

(a) Comparison between α measurements.

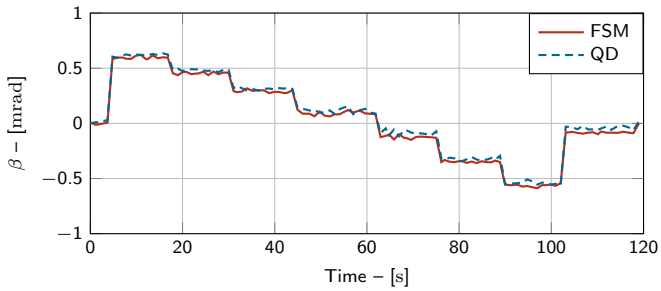

(b) Comparison between β measurements.

Fig. 10 Comparison of values of α and β calculated from the FSM strain gauges measurements and the QD outputs according to Eq. 7, after the calibration of the optical system.

ground station or a remote terminal. When the QD inside the MOS detects the beacon beam, LaserCube switches to tracking mode and aligns its boresight with the direction of the incoming beam.

The beacon acquisition phase is critical, especially in the case of DL communication. The contact time between the spacecraft and the ground station is limited and the acquisition of the reference beacon can take a relevant portion of the available time. An efficient acquisition procedure maximises the time available for data transmission over the optical link. A spiral trajectory is adopted to quickly detect the incoming beacon and its capability to effectively acquire the beam is verified in this section.

1. Spiral Search

The scanning trajectory executed during the seeking procedure follows a simple Archimedean spiral trajectory in the $[\vartheta, \psi]$ space. The initial position is the point $[0, 0]$ that corresponds to the null position of the coarse pointing mechanism. The spiral is described by three parameters: the spiral pitch, the spiral maximum radius and the spiral velocity. In polar coordinates, the current value of the spiral radius is proportional to the cumulative angle swept since the initial time. The spiral pitch is the radius increment occurred between two consecutive revolutions. Once the spiral radius reaches the maximum value, the sign of the radius variation is inverted, i.e., the spiral motion continues with decreasing radius. When the radius falls below a minimum threshold, the sign of its variation is inverted again, and so on. Both the spiral pitch, maximum radius and velocity are configuration parameters of the LaserCube flight model that

can be modified through telecommands.

In order to execute the spiral motion, the spiral trajectory current position $[\vartheta(t), \psi(t)]$ at the time t is calculated by the LaserCube microcontroller with an update rate of 100 Hz. At each step, the angular position is converted to a linear setpoint for the SPIN linear motors $[L_{1ref}, L_{2ref}]$ (see Fig. 3). Two Proportional–Integrative (PI) controllers (one for each linear motor) perform close–loop control of the linear actuator velocities using the linear motors position given by the encoders as feedback (inner loop in Fig. 3). An example of spiral search trajectory is presented in Fig. 11a, showing the inversion of the radius variation; the measured orientation $[\vartheta, \psi]$ of the SPIN upper platform is calculated by applying the direct kinematic conversion on the elongation of the linear actuators given by the encoders.

2. Beacon Acquisition and Loss

The beacon acquisition functionality has been tested with the test setup shown in Fig. 4. The attenuated laser (1 μW) sent through the beam expander is switched on/off to simulate the presence/absence of the beacon beam used as the tracking reference. When the beacon laser is turned off, LaserCube loses the tracking reference and switches to acquisition mode, immediately starting the seeking trajectory (spiral). After the beacon laser is switched on, LaserCube easily detects the direction of the incoming beam and switches back to tracking mode. When in tracking mode, the dual stage pointing system locks on the beacon signal provided by the QD and aligns itself with the direction of the incoming laser, minimizing the pointing error. The system behaviour in case of beacon loss/acquisition is verified by repeatedly switching on/off the beacon beam and by recording the elongation of the SPIN linear motors; the elongations are then converted into $[\vartheta(t), \psi(t)]$ angles through the direct kinematic function. This test allows the verification of the correct detection of the laser by the QD and the automatic switching from acquisition mode to tracking mode and viceversa.

Figure 11b shows the trajectory swept during the test in the $[\vartheta(t), \psi(t)]$ domain. The QD output voltages are shown in Fig. 12. The sum voltage of the QD outputs is close to zero (laser beacon off) when the OMU performs the spiral search; differently, the sum voltage is maximum (> 1 V, laser beacon on) when the system correctly detects the beacon laser, switches to tracking mode and aligns its boresight with the beacon direction. Figure 13 shows a test sequence with three subsequent activations/deactivations of the beacon laser: the $[\vartheta(t), \psi(t)]$ angles are virtually null when the beacon is on and LaserCube is in tracking mode (voltage sum is high); the angles vary periodically when the system is in acquisition mode (voltage sum is low). Pointing is recovered in less than 5 s after the QD detects the beam.

D. Pointing and Tracking

This section reports the results of the tracking tests carried out imposing a perturbation profile at the base of the OMU by means of the pan–tilt platform. Sinusoidal perturbations are applied with a given combination of amplitude and frequency. The reference disturbance profile can be found in [15, 18, 19]. For this test campaign, the disturbance profile was partially relaxed considering the expected filtering effects of the structure of the satellite that hosts LaserCube

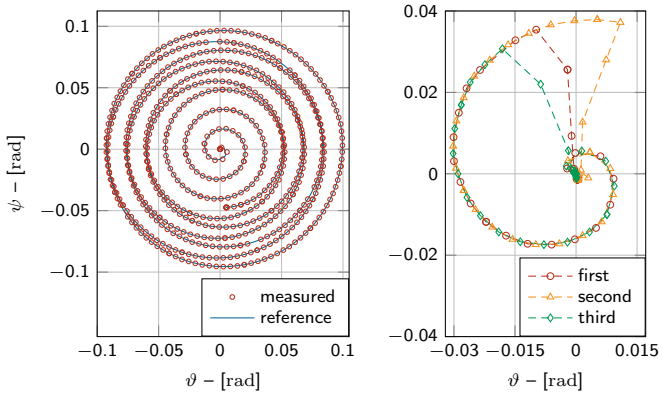

(a) (b)

Fig. 11 Spiral search (a) and repeated transitions to tracking mode (b) after the beacon power-up during the test sequence.

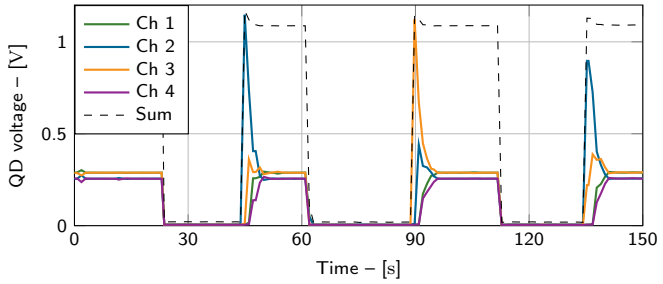

Fig. 12 Output voltages of the QD during the acquisition test sequence (four channels and sum).

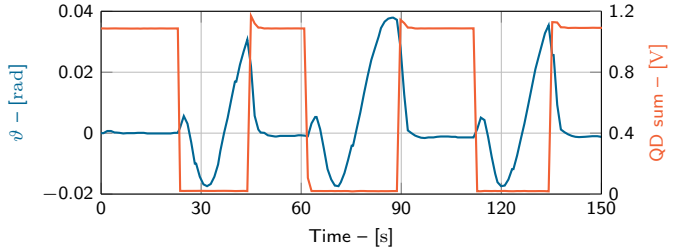

(a) Elevation (ϑ)

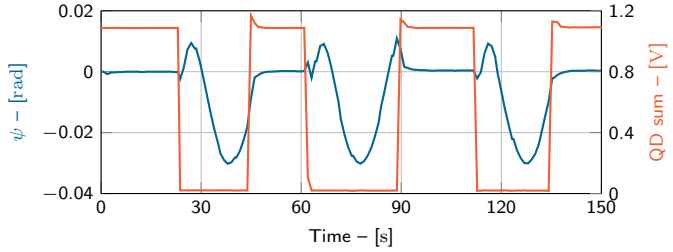

(b) Azimuth (ψ)

Fig. 13 System monitoring during three subsequent search and detection tests: the plot shows the pointing angles (red) and the sum of the four QD outputs (blue).

Frequency [Hz]	Amplitude [µrad]	σ_ψ [µrad]	σ_ϑ [µrad]
0	0 (static)	2.5	2.2
0.005	17000	3.9	7.3
0.05	1000	3.5	9.2
3	50	2.8	3.9

Table 2 Summary of tracking tests results with dynamic perturbations.

during its in–orbit demonstration. In order to measure the pointing error of the system during tracking, the telecom laser sent by LaserCube through the beam expander is focused on the external PSD as shown in Fig. 4. The PSD measures the linear motion of the laser spot on the detector sensitive area. The spot position is then correlated to the alignment error of the laser beam in a similar fashion to what described in Sec. III.B.1 relatively to the QD. The resulting pointing accuracy is expressed in terms of standard deviation of the pointing error along the azimuth and elevation axes (σ_ψ and σ_ϑ, respectively). The test procedure is the following:

1) Turn on the FM of LaserCube–DL.
2) Warm–up of the terminal and all support electronics (the warm–up time is ~ 150 s).
3) Turn on the beacon laser.
4) Start of the seeking procedure.
5) Detection of the beacon laser by the QD and automatic transition to tracking mode.
6) Command the pan–tilt disturbance motion by imposing pre–set sinusoidal motion.
7) Measure the motion of the telecom laser spot by means of the PSD.

Pointing accuracy was also measured in static conditions, i.e., without any perturbation imposed by the pan–tilt stage. In this case, the pointing error is slightly larger than the uncertainty of the $[\vartheta(t), \psi(t)]$ static values estimated by the sole QD (see Sec. III.B.1), meaning that, in absence of an external disturbance, the QD noise is the major contributor to the error budget. The pointing error along azimuth and elevation estimated by PSD measurements for each test is shown Tab. 2. The pointing error is always below 10 µrad rms.

IV. Conclusions

This paper presents the ground calibration and experimental verification of the pointing, acquisition and tracking system of the flight model of LaserCube–DL, which is a miniature optical communication terminal for nano and micro satellites. LaserCube is conceived to provide small satellites (6 U CubeSat factor and larger) unprecedented communication capabilities either in direct to Earth links (1 Gbps) or in intersatellite links (100 Mbps). The adoption of LaserCube terminals on–board small satellites for earth observation and / or data relay constellations in LEO will lead to a dramatic decrease of data latency and an increased availability of data to the final users. This is accomplished by exploiting a combination of high–throughput downlinks to ground stations and the possibility to route data throughout

the constellation thanks to intersatellite connectivity. The first LaserCube flight model for downlink applications was launched in June 2021 on board the D–Orbit ION Satellite Carrier 003 for its In–Orbit Demonstration mission that is currently ongoing at the time of writing.

First, the calibration process of critical parameters of the control algorithm of the dual–stage pointing system is described. Then, the paper presents the validation of the beacon acquisition process; experimental results show the capability of the system of detecting low–power laser beams sent by a remote terminal and recover from beacon loss in less than 5 s. Finally, dynamic tracking of the beacon laser under environmental disturbances has been tested; results show that the LaserCube PAT system is capable of maintaining pointing accuracy below 10 µrad rms under external disturbances.

Funding Sources

This work is supported by the Italian Space Agency in the framework of the ESA ARTES C&G program.

References

[1] Janson, S., Welle, R., Rose, T., Rowen, D., Hardy, B., Dolphus, R., Doyle, P., Faler, A., Chien, D., Chin, A., Maul, G., Coffman, C., La Lumondiere, S. D., Werner, N. I., and Hinkley, D., "The NASA Optical Communications and Sensor Demonstration program: initial flight results," *30th Annual AIAA/USU Conference on Small Satellites*, 2016.

[2] Rose, T. S., Rowen, D. W., LaLumondiere, S., Werner, N. I., Linares, R., Faler, A., Wicker, J., Coffman, C. M., Maul, G. A., Chien, D. H., Utter, A., Welle, R. P., and Janson, S. W., "Optical communications downlink from a 1.5U Cubesat: OCSD program," *International Conference on Space Optics — ICSO 2018*, Vol. 11180, edited by Z. Sodnik, N. Karafolas, and B. Cugny, International Society for Optics and Photonics, SPIE, 2019, pp. 201 – 212. doi:https://doi.org/10.1117/12.2535938.

[3] Payne, C., Aguilar, A., Barnes, D., Diez, R., Kusters, J., Grenfell, P., Aniceto, R., Sackier, C., Allan, G., and Cahoy, K., "Integration and testing of the Nanosatellite Optical Downlink Experiment," *32nd Annual AIAA/USU Conference on Small Satellites*, 2018.

[4] Čierny, O., and Cahoy, K. L., "On–orbit beam pointing calibration for nanosatellite laser communications," *Optical Engineering*, Vol. 58, No. 04, 2018, p. 1. doi:https://doi.org/10.1117/1.oe.58.4.041605.

[5] Serra, P., Cierny, O., Diez, R., Grenfell, P., Gunnison, G., Kammerer, W., Kusters, J., Payne, C., Murphy, J., Sevigny, T., do Vale Pereira, P., Yenchesky, L., Cahoy, K., Clark, M., Ritz, T., Coogan, D., Conklin, J., Mayer, D., Hanson, J., and Stupl, J., "Optical Communications Crosslink Payload Prototype Development for the Cubesat Laser Infrared CrosslinK (CLICK) Mission," *33rd Annual AIAA/USU Conference on Small Satellites*, 2019.

[6] Grenfell, P., Serra, P., Cierny, O., Kammerer, W., Gunnison, G., Kusters, J., Payne, C., Cahoy, K., Clark, M., Ritz, T., Coogan, D., Conklin, J., Mayer, D., Stupl, J., and Hanson, J., "Design and prototyping of a nanosatellite laser communications terminal forthe Cubesat Laser Infrared CrosslinK (CLICK) B/C mission," *34th Annual AIAA/USU Conference on Small Satellites*, 2020.

[7] Cierny, O., Serra, P., Kammerer, W., Grenfell, P., Gunnison, G., Kusters, J., Payne, C., do Vale Pereira, P., Cahoy, K., Ritz, T., Conklin, J., Mayer, D., Stupl, J., and Hanson, J., "Testing of the cubesat laser infrared crosslink (CLICK–A) payload," *34th Annual AIAA/USU Conference on Small Satellites*, 2020.

[8] Fuchs, C., Schmidt, C., Keim, J., Moll, F., Rödiger, B., Lengowski, M., Gaißer, S., and Giggenbach, D., "Update on DLR's OSIRIS program and first results of OSIRISv1 on Flying Laptop," *Proc. of SPIE*, Vol. 10910, 2019. doi:https://doi.org/10.1117/12.2514349.

[9] Schmidt, C., Rödiger, B., Rosano, J., Papadopoulos, C., Hahn, M.-T., Moll, F., and Fuchs, C., "DLR's Optical Communication Terminals for CubeSats," *2022 IEEE International Conference on Space Optical Systems and Applications (ICSOS)*, 2022, pp. 175–180. doi:https://doi.org/10.1109/ICSOS53063.2022.9749735.

[10] Storm, M., Gupta, S., Cao, H., Litvinovitch, S., Puffenberger, K., Albert, M. M., Young, J., Pachowicz, D., and Deely, T., "Cubesat Laser Communications Transceiver for Multi-Gbps Downlink," *31st Annual AIAA/USU Conference on Small Satellites*, 2017.

[11] Mathason, B., Albert, M. M., Engin, D., Cao, H., Petrillo, K. G., Hwang, J., Le, K., Puffenberger, K., Litvinovitch, S., Storm, M., and Utano, R., "CubeSat lasercom optical terminals for near-Earth to deep space communications," *Free-Space Laser Communications XXXI*, Vol. 10910, edited by H. Hemmati and D. M. Boroson, International Society for Optics and Photonics, SPIE, 2019, pp. 24 – 29. doi:https://doi.org/10.1117/12.2508047.

[12] "CubeCat, AAC Hyperion," , 2022. URL `https://www.aac-clyde.space/what-we-do/space-products-components/communications/cubecat`.

[13] "Stellar Project," , 2022. URL `https://stellarproject.space/`.

[14] Sansone, F., and Francesconi, A., "Compact stabilized pointing system," WO2017115204A1, 2017.

[15] Sansone, F., Branz, F., Vettor, A., and Francesconi, A., "Acquisition Analysis for Small-Satellite Optical Crosslinks," *2021 IEEE 8th International Workshop on Metrology for AeroSpace (MetroAeroSpace)*, 2021, pp. 412–417. doi:https://doi.org/10.1109/MetroAeroSpace51421.2021.9511705.

[16] Kobayashi, M., and Horowitz, R., "Track seek control for hard disk dual-stage servo systems," *IEEE Transactions on Magnetics*, Vol. 37, No. 2, 2001, pp. 949–954. doi:https://doi.org/10.1109/20.917648.

[17] Horowitz, R., Li, Y., Oldham, K., Kon, S., and Huang, X., "Dual–stage servo systems and vibration compensation in computer hard disk drives," *Control Engineering Practice*, Vol. 15, No. 3, 2007, pp. 291–305. doi:https://doi.org/10.1016/j.conengprac.2006.09.003.

[18] Antonello, R., Branz, F., Sansone, F., Cenedese, A., and Francesconi, A., "High–Precision Dual–Stage Pointing Mechanism for Miniature Satellite Laser Communication Terminals," *IEEE Transactions on Industrial Electronics*, Vol. 68, No. 1, 2021, pp. 776–785. doi:https://doi.org/10.1109/TIE.2020.2972452.

[19] Sansone, F., Francesconi, A., Corvaja, R., Vallone, G., Antonello, R., Branz, F., and Villoresi, P., "LaserCube optical communication terminal for nano and micro satellites," *Acta Astronautica*, Vol. 173, 2020, pp. 310–319. doi:https://doi.org/10.1016/j.actaastro.2020.04.049.